Improving Device Design in Insulator-Based Electrokinetic Tertiary Separations

Alaleh Vaghef-Koodehi,[†] Patricia Cyr,[a] and Blanca H. Lapizco-Encinas[†,*]

[†] Microscale Bioseparations Laboratory and Biomedical Engineering Department, Rochester Institute of Technology, 160 Lomb Memorial Drive, Rochester, New York, 14623, United States.

[a] Department of Industrial and Systems Engineering, Rochester Institute of Technology, 160 Lomb Memorial Drive, Rochester, New York, 14623, United States.

*Email: bhlbme@rit.edu

Keywords:

Electrokinetic

Electrophoresis

Microfluidic

Microparticle

Separations

ABSTRACT

This study presents a methodology for designing effective insulator-based electrokinetic (iEK) systems for separating tertiary microparticle samples, which can be extended to more complex samples. First, 144 distinct iEK microchannel designs were built considering different shapes and arrangements of the insulating posts. Second, a mathematical model was developed with COMSOL software to predict the retention time of each particle type in the microchannel, this allowed identifying the best channel designs for two distinct types of separations: charge-based and sized-based. Third, the experimental charge-based and size-based separations of the tertiary microparticle mixtures were performed employing the improved designs identified with COMSOL modeling. The experimental results demonstrated successful separation in terms of separation resolution and good agreement with COMSOL predictions. The findings from this study show that the proposed method for device design, which combines mathematical modeling with varying post shape and post arrangement is an effective approach for identifying iEK systems capable of separating complex microparticle samples.

Numerous traditional methods, such as capillary electrophoresis (CE) and chromatography, are available to analyze nano-sized bioparticles. However, not many efficient analogous techniques exist for analyzing micron-sized particles, including microorganisms.[1] Microfluidic systems have been successfully employed to study nano- and microparticles of interest.[1,2] Electrokinetic (EK) techniques are a major pillar in the field of microfluidics.[2,3] In particular, insulator-based EK (iEK) systems have gained recent attention due to their simplicity and robustness and their unique capability of combining linear and nonlinear EK effects within the same device. In these systems insulating structures embedded within a microchannel alter the electric field distribution, resulting in the development of higher electric field intensity zones that enable the rise of nonlinear EK effects. Employing iEK devices has enabled the separation of complex samples, including bioparticles ranging from macromolecules to mammalian cells.[4–6]

As real-life particle samples are inherently complex, techniques able to handle samples with more than two components are needed. The existing reports on tertiary separations of particles underscore the significance of studying complex samples. These studies have continuous size-selective separation of microparticles of different sizes[7] and AC potentials.[8,9] Our group studied the separation of tertiary samples of polystyrene particles, bacterial and yeast cells employing iEK devices stimulated with a DC potentials[10] and DC-biased low-frequency AC potentials.[11]

The flexibility of iEK systems, which allows for combining linear and nonlinear EK effects, makes them attractive platforms for particle and cell analysis. Several groups have reported the use of iEK systems to separate particles and cells by exploiting size and/or charge differences.[8,12–16] However, the omission of nonlinear electrophoresis (EP_{NL}) in these previous studies,[8,12–16] led to the utilization of correction factors for reconciling experimental and modeling results.[17] Several past studies[13,18,19] have focused on the impact of the shape of the insulating posts on particle trapping and separation, however these reports were influenced by correction factors as the effects of EP_{NL} were not considered; thus, an updated analysis on the effect of post shape considering EP_{NL} is needed.

Recent reports, supported by the new advances in the strong-field theory during the last decade,[20] unveiled the importance of EP_{NL} in iEK systems.[21–23] Utilizing EP_{NL} enables separations by exploiting shape and size differences, which are not feasible with traditional methods, such as linear electrophoresis (EP_L).[24,25] There has been a recent surge of studies on the migration of particles and cells under EP_{NL},[21–23,26–31] including reports on the charge-based separation of almost identical polystyrene microparticles,[30] and the separation of binary mixtures of particles and cells under DC potential.[31]

This study proposes a method for iEK device design under DC potentials for separating tertiary samples of microparticles based on charge and size differences by combining modeling and experimentation. COMSOL

Multiphysics was utilized to predict the retention time of particles in the iEK device. The main objective of the design improvement process was to increase the differences in predicted particle retention times ($\Delta t_{R,p}$). A total of 144 distinct channel designs were created by varying the post shape and spacing. Results indicated that for performing charge-based separations, the best design (highest $\Delta t_{R,p}$) was Oval-Square shaped posts with a horizontal length of 250 μm, and horizontal spacing of 200 μm. For size-based separation the best design was Oval-Square shaped posts with a horizontal post length of 300 μm and horizontal spacing of 100 μm. Experimental separation results were evaluated by calculating the separation resolution (*Rs*) and the number of plates (*N*). The experimental results were in good agreement with the modeling results. The findings from this study demonstrate that the proposed device design method, that, varies post shape and post arrangement, is effective for identifying iEK systems capable of separating complex microparticle samples

THEORY

Four EK phenomena are considered in this study: linear electrophoresis (EP_L), nonlinear electrophoresis (EP_{NL}), electroosmotic (EO) flow and dielectrophoresis (DEP). The velocity expressions for these phenomena are included in the supporting material. Considering these four EK phenomena, the overall particle velocity ($\mathbf{v}_P$) becomes:

$$\mathbf{v}_P = \mathbf{v}_{EO} + \mathbf{v}_{EP,L} + \mathbf{v}_{DEP} + \mathbf{v}_{EP,NL}^{(3)} \qquad (1)$$

where $\mathbf{v}_{EP,NL}^{(3)}$ represents the EP_{NL} velocity with a cubic dependence with **E**. To assess the quality of each of the tertiary separations the parameters separation resolution (*Rs*) and number of plates (*N*) were employed. Details on these parameters are in the supporting material.

EXPERIMENTAL SECTION

Microparticle Samples and Suspending Medium. This study employed six distinct types of polystyrene microparticles purchased from Magsphere and Spherotech (**Table 1**). The suspending media was a buffer solution of K_2HPO_4 at a 0.2 mM concentration, with the addition of 0.05% (v/v) of Tween 20 to prevent particle sticking. The media had a conductivity was 41 ± 4.0 μS/cm with a pH of 7.3 ± 0.5, which produced a wall zeta potential (ζ_W) of -60.1 ± 3.7 mV as measured with current monitoring.[32]

Table 1. Characteristics of the microparticles used in this study.

ID and color	Diameter (μm)	Surface functionalization	ζ_P (mV)	$\mu_{EP,L}$ x 10^{-8} ($m^2V^{-1}s^{-1}$)	E for $\mu_{EP,NL}^{(3)}$ estimation (V/cm)	$\mu_{EP,NL}^{(3)}$ x 10^{-18} ($m^4V^{-3}s^{-1}$)
Particle 1, red	5.8 ± 0.2	Carboxylated	-20.5 ± 2.2	-1.6 ± 0.1	150	-25.2 ± 6.7
Particle 2, green	5.7 ± 0.2	Non functionalized	-34.1 ± 3.7	-2.6 ± 0.1	150	-16.1 ± 1.1
Particle 3, blue	5.5 ± 0.3	Carboxylated	-42.1 ± 2.7	-3.2 ± 0.2	100	-15.1 ± 8.2
Particle 4, green	4.1 ± 0.3	Carboxylated	-19.1 ± 3.2	-1.5 ± 0.1	350	-2.1 ± 1.8
Particle 5, red	7.4 ± 0.3	Carboxylated	-31.8 ± 1.8	-2.5 ± 0.1	100	-7.3 ± 5.3
Particle 6, blue	11.7 ± 0.2	Non functionalized	-23.8 ± 1.1	-1.9 ± 0.1	100	-23.2 ± 16.7

Microdevices and Equipment. Standard cast-molding techniques were employed to create the T-channel devices used in this work (**Fig. 1a)**. Samples were introduced using a three-step EK sample injection process.[33] All experiments were recorded employing two inverted microscopes, a Zeiss Axiovert 40 CFL and a Leica DMi8. A

LabSmith high-voltage power supply (model HVS6000D) was used to apply the voltage sequences to the microchannels.

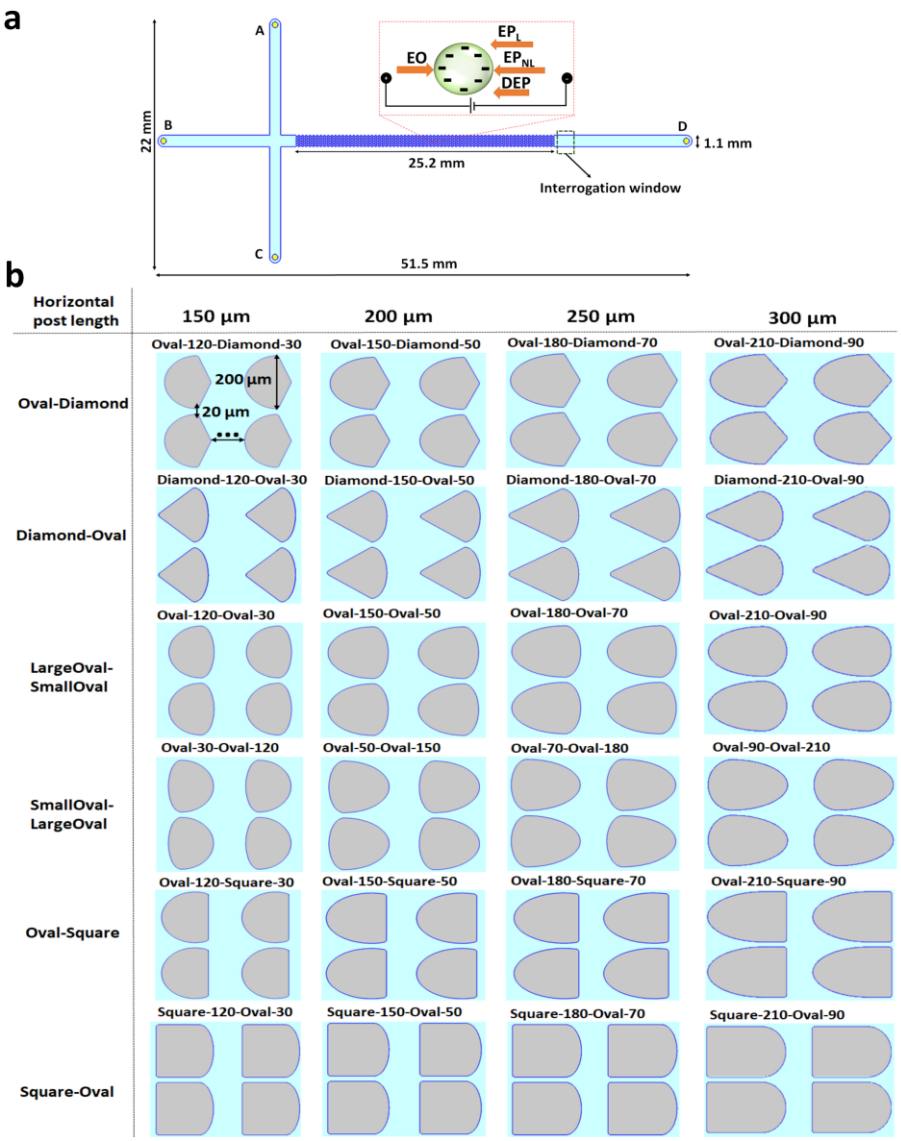

Figure 1. Representation of a T-cross iEK microchannel and the distinct post configurations modeled with COMSOL. **a)** Illustration of the microchannel and its dimensions. The labels A−D refer to the location of the four electrodes. The inset is a representation of the four EK forces (EO, EP_L, EP_{NL}, and DEP) exerted on particles. **b)** Representation of the 144 distinct shapes of insulating posts employed in this work organized by post horizontal length. The horizontal spacing between insulating posts, which is shown as ⇿, varies between 50-300 µm (**Table 2**). All vertical spacing between posts is 20 µm.

Mathematical Modeling. Predictions of particle retention time ($t_{R,p}$) were obtained with a COMSOL *Multiphysics* model. For predicting $t_{R,p}$, microparticle characteristics were first obtained by particle tracking velocimetry (PTV) measurements[26–28] (**Table 1**). The variables studied to build the distinct iEK configurations and identify the most improved designs are listed in **Table 2**. COMSOL modeling was also used to identify the appropriate voltages needed in each tertiary separation to achieve a Rs > 1.5. Details on the COMSOL model, and modeling results are in **Figures S1-S2,** and **Tables S2-S4.**

Table 2. Variables employed to identify the most improved device designs for each separation process.

Variable	Study	Description or values of the variables
Post shape	Charge-based separation and size-based separation	Oval-Diamond, Diamond-Oval, LargeOval-SmallOval, SmallOval-LargeOval, Oval-Square, and Square-Oval
Horizontal post length	Charge-based separation and size-based separation	150 μm, 200 μm, 250 μm, and 300 μm.
Horizontal spacing between posts	Charge-based separation	150 μm, 200 μm, 250 μm, and 300 μm.
	Size-based separation	50 μm, 100 μm, 150 μm, 200 μm, 250 μm, and 300 μm.

Experimental Procedure. Experimental work was carried out in two parts: PTV experiments were used to characterize the particles and then after identifying appropriate operating conditions with the model, separation experiments were performed employing the voltages in **Table 3**. Further details on the PTV experiments and separation experiments are in the supporting material.

RESULTS AND DISCUSSION

Improved Device Design for the Charge-Based Separation of a Tertiary Sample

Charge-based separations require low voltages to ensure that EP_L is the discriminatory EK mechanism driving the separation, since EP_L differentiates particles by charge, but cannot differentiate particles by size or shape.[20,24,25] To identify a device design suitable for charge-based separations, the first step was performing COMSOL simulations considering particles IDs # 1-3 with diameters between 5.5-5.8 μm and ζ_P from -20.5 to -42.1 mV (**Table 1**). A total of 96 COMSOL models were built considering the T-cross iEK microchannel in **Figure 1a** and the distinct post arrangements illustrated in **Figure 1b** and listed in **Table 2**. The models considered four horizontal post lengths (150, 200, 250, 300 μm), and four horizontal spacings between insulating posts (150, 200, 250, 300 μm). The models were used to estimate $t_{R,p}$ for particles in the 96 designs under 350 V (**E**= 43.3 V/cm) between electrodes B-D, which is the minimum voltage required for the EK injection to occur. The results in **Figure 2** illustrate the mean difference between the retention time between the particles, $\overline{\Delta t}_{R,p}$. It is seen in **Figure 2a** that the post shapes of Square-Oval and Oval-Square result in higher $\overline{\Delta t}_{R,p}$ values, indicating better discrimination capabilities. Under weak field conditions, particle separation is mainly driven by EP_L, and particle elution is determined by the ζ_P values, where particles with a higher magnitude in ζ_P have a lower overall migration velocity, as EP forces are towards the inlet for the negatively charged particles in this study. Thus, the elution order is as follows, red particles (ζ_P = –20.5 mV) first, green particles (ζ_P = –34.1 mV) second, and blue particles (ζ_P = – 42.1 mV) last. **Figures 2b-2e** further confirm that larger differences between ζ_P values lead to larger difference between $t_{R,p}$ values. **Figure 2b** illustrates that higher horizontal spacing between posts increases the $\overline{\Delta t}_{R,p}$ values, enhancing the discriminatory capabilities of the device. A similar result is observed in **Figure 2c**, where posts length of 200-250 μm produce higher $\overline{\Delta t}_{R,p}$ values, however, no significant increase in $\overline{\Delta t}_{R,p}$ was observed for horizontal post lengths above 250 μm. **Figures 2d-2e** show the $\Delta t_{R,p}$ predictions for the first-best option and second-best option designs, which are named Square-150-Oval-50-VS20-HS300 and Oval-180-Square-70-VS20-HS200, respectively. Designs names follow a naming convention that lists the asymmetric post shapes and their individual horizontal length, followed by the vertical spacing (VS) and horizontal spacing (HS) values.

In summary, the results in **Figure 2** demonstrated that longer posts (200 μm and beyond) produce an increase in $\Delta t_{R,p}$ values as longer posts allow for longer migration distances, resulting in better discriminatory capabilities by exploiting differences in particle migration velocity. This is analogous to employing a longer column in chromatographic separations. These results also unveiled that increasing the horizontal spacing between posts

results in better charge-based particle separations as fewer columns of posts are present in the fixed-length post array. Fewer columns of posts results in a higher voltage drop at each column, resulting in stronger electric fields at the constriction regions between the posts; making each column of posts "more effective" for separation purposes, as demonstrated in a previous sudy.[34]

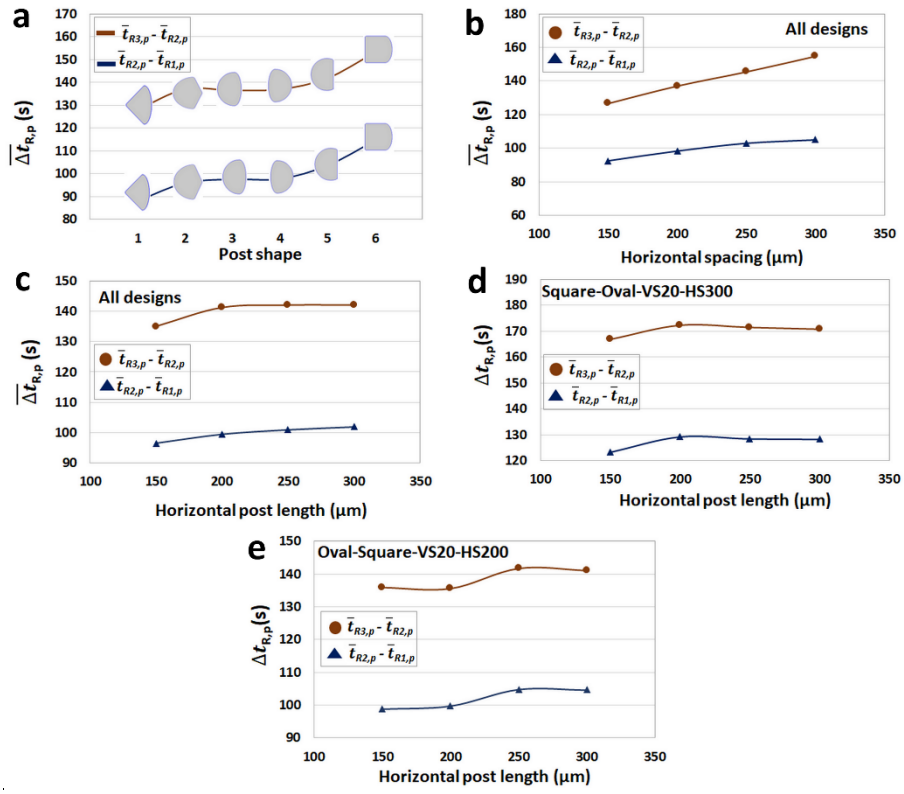

Figure 2. COMSOL predictions for the charge-based separation under ΔV = 350 V between electrodes B and D. **a)** Plot of difference in retention time of particles ($\overline{\Delta t}_{R,p}$) for the six distinct post shapes, showing that Square-Oval and Oval-Square configurations yield the best $\overline{\Delta t}_{R,p}$ values. **b)** Plot of $\overline{\Delta t}_{R,p}$ for all designs as a function of the horizontal spacing between posts. **c)** Plot of $\overline{\Delta t}_{R,p}$ for all designs as a function of the horizontal post length. **d)** Plot of the $\Delta t_{R,p}$ values obtained for the first-best option design, Square-Oval-VS20-HS300, showing that a horizontal post length of 200 µm results in the highest $\Delta t_{R,p}$ value. **e)** Plot of the $\Delta t_{R,p}$ values obtained for the second-best option design, Oval-Square-VS20-HS200, showing that a horizontal post length of 250 µm results in the highest $\Delta t_{R,p}$ value.

Experimental Charge-Based Separation of a Tertiary Sample Using the Improved Device

First, the design identified as the first-best option (Square-150-Oval-50-VS20-HS300) was utilized to perform experimental charge-based separation of particles ID 1-3, (**Table 1**). The experimental results under a range of voltages ($\Delta V = 350$ V to 1000 V) demonstrated that the Square-150-Oval-50-VS20-HS300 configuration induces trapping for the 5.5 µm blue particles, which possesses the highest magnitude zeta potential ($\zeta_P = -42.1$ mV). This trapping effect prevented the elution of 5.5 µm blue particles, making the continuous separation of the particles impossible under these experimental conditions. While this configuration was identified as highly efficient in COMSOL simulation in terms of $t_{R,p}$ values, the experimental results in terms of $t_{R,e}$ revealed that design Square-150-Oval-50-VS20-HS300 is excessively improved, leading to a strong emergence of EP_L effects on the particles with the highest magnitude of ζ_P, resulting in them being trapped.

Subsequently, the second-best improved design (Oval-180-Square-70-VS20-HS200, shown in **Figure 3a**) was the one employed for the experimental charge-based separation of the particles sample. COMSOL predictions were carried out (**Table S3**) to identify the best voltage values for this separation to obtain separated peaks ($Rs > 1.5$),

the selected voltages are listed in **Table 3**. Further details for COMSOL modeling are reported in **Figures S1-S2** and **Table S2**. The images in **Figures 3b-3c** show the particles as they migrate across the post array under $\Delta V = 400\ V$ (**E**= 54.8 V/cm) where "zones" are observed for each distinct particle type with the following elution order, red first, then green, and last the blue particles. The electropherogram in **Figure 3d** illustrates three separated peaks which were obtained from the fluorescence signal from the particles as they passed through the interrogation window in **Figure 1a**. These results are as expected, as EP_L is the discriminatory EK effect driving the separation at the low electric field employed, which allowed exploiting differences in ζ_P values in this charge-based particle separation. The red particles possess the lowest magnitude in ζ_P, thus, they have a highest overall velocity ($\mathbf{v}_P$). The $t_{R,e}$ values, which depend directly on ζ_P values, are 208, 298 and 347 s for red, green and blue particles, respectively. This separation had resolutions of Rs = 2.61 between the red and green particles and Rs = 1.42 between the green and blue particles. The separation efficiency in terms of plates per meter were 18,060, 9,492, and 50,263 plates/m for the red, green, and blue particles, respectively; which are comparable to those obtained with conventional capillary electrophoresis systems.[35] The variation between experimental repetitions was below 6% (**Table 4** and **Table S5**). The velocity estimations for each particle are included in **Figure S3a-c**, depicting the relative effect of each one of the four EK phenomena considered here: EO, EP_L, EP_{NL} and DEP.

Regarding the agreement between modeling and experimental results, **Table 4** shows the experimental ($t_{R,e}$) and predicted ($t_{R,p}$) retention time values for all the particles under $\Delta V = 400\ V$ (**E**= 54.8 V/cm), where deviations below 24% between COMSOL predictions and experimental results were obtained in all cases. The COMSOL model utilized here does not require the use of any correction factors[17,30] to be in fair agreement with experiments. The modeling results, although with deviations, represent a valuable tool for identifying suitable experimental conditions. A potential cause for these deviations could be "injection bias" during the EK sample injection method, as injection bias would accelerate the particles with higher migration velocity.[36] Another potential deviation cause could be particle-particle interactions caused by the high particle concentration in the sample, since particles themselves distort the local electric field distribution.[37] Also, it is worth mentioning that the model employed here only mimics the last step of the separation process; that is, the model does not consider potential deviation in steps one and two of the EK injection process. These results obtained here with the proposed device design process represent a step forward in iEK separations devices, as previous reports did consider the effects of EP_{NL} on particle migration.[13,19] Although EP_L is the main discriminatory EK mechanism driving the separation, considering the effects of EP_{NL} makes the model more accurate, since EP_{NL} are present and need to be considered.

Table 3. Voltages and concentration of the particle samples employed for EK sample injection and iEK-based separations.

Separation ID	Description	Particle concentration x 10^8 (#/mL)	Step	Run time (s)	Applied voltage (V) at each reservoir			
					A	B	C	D
1	Charge-based separation: red (5.8 µm), green (5.7 µm), and blue (5.5 µm)	Red: 1.3 Green: 1.3 Blue: 0.6	Loading	12	1500	100	0	1000
			Gating	4	1500	1500	1500	0
			Injection	550	200	400	200	0
2	Size-based separation: green (4.1 µm), red (7.4 µm), and blue (11.7 µm)	Green: 0.6 Red: 0.3 Blue: 0.1	Loading	30	1500	100	0	1000
			Gating	6	1500	1500	1500	0
			Injection	500	200	1500	200	0

Table 4. Modeling and experimental separation results, deviation values are from three repetitions.

Separation ID	Particle ID	Rs Particles 1&2 / 4&5	Rs Particles 2&3 / 5&6	COMSOL predicted $t_{R,p}$ (s)	Exp. $t_{R,e}$ (s)	Deviations in $t_{R,p}$ vs. $t_{R,e}$ (%)	Deviation in repetitions (%)
1	Particle 1, red	2.61	1.42	192.7	208	7	5
	Particle 2, green			291.4	298	2	5
	Particle 3, blue			427.2	347	-23	3
2	Particle 4, green	3.06	3.69	63.2	50	-26	7
	Particle 5, red			103.9	125	17	18
	Particle 6, blue			NA	254	NA	14

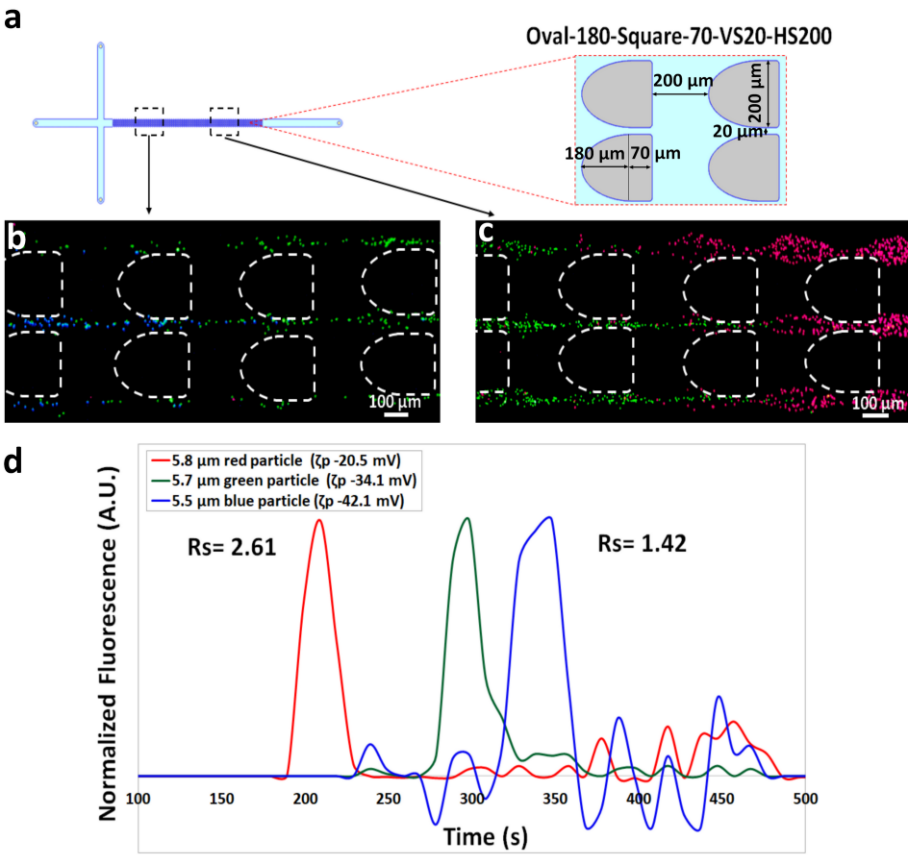

Figure 3. Experimental results for the charge-based separation. **a)** Illustration of the device. **b-c)** Particles as they migrate across the post array in the following order: red first, then green, with the blue particles migrating last. **d)** Electropherogram depicting the three particle peaks. A video of this separation is included as supplementary information as **Video_S1.mp4**. Results were obtained under ΔV = 400 V.

Improved Device Design for the Size-Based Separation of a Tertiary Sample

To select a device design for a size-base separation, higher voltages are required to engage the mechanism of EP_{NL}, which can discriminate particles by size or shape, as size or shape-based separations are not possible with EP_L as the discriminatory mechanism.[20,24,25] Similar to the design process for the charge-based separation, the first step was to perform COMSOL simulations to predict $t_{R,p}$ for particles IDs # 4-6 with diameters (4.1, 7.4 and 11.7 µm) and similar ζ_P values ranging from -19.1 to -31.8 mV (**Table 1**). Additional data on the EP_{NL} velocity of the particles

is in **Table S1**. A total of 144 channel designs were built, considering six post shapes (**Figure 1b**), four horizontal post lengths (150, 200, 250, 300 µm), and six horizontal spacings between insulating posts (50, 100, 150, 200, 250, 300 µm) as shown in **Table 2**. In the nonlinear regime, particle elution order is determined by EP_{NL} forces, where a larger magnitude of $\mu_{EP,NL}^{(3)}$ leads to later elution. Particles with larger sizes have a larger magnitude in their $\mu_{EP,NL}^{(3)}$ value, as demonstrated by previous studies.[26,38] Consequently, the size-based separation process should result in the following elution order: first 4.1 µm green, followed 7.4 µm red, and 11.7 µm blue particles last. Since higher applied voltages are required for EP_{NL} effects, the maximum possible electric fields for all configurations were explored. **Figure 4a**, which contains a plot of post shape vs. the max **E** field that can be applied before producing particle trapping, shows that only Square-Oval and Oval-Square post shapes are functional under high max **E** fields, all other post shapes produce particle trapping, hindering the continuous separations process. For both of these shapes a horizontal spacing (HS) of 100 µm was the most effective. To achieve a size-based separation it was necessary to ensure that the **E** field was high enough for EP_{NL} effects to be significant, so the particles would elute in the order of increasing size (green, red, and blue), otherwise, under low voltages, EP_L is the discriminatory mechanism and the separation would be charge-based. Due to their ζ_P values, the elution order between the blue and red particles (IDs # 6 and 5) is the parameter to be studied to ensure a size-based separation, while making sure that the $\Delta t_{R,p}$ between particles IDs # 5 and 4 remains above 40 s, which the minimum required, observed experimentally, to achieve resolved peaks (Rs > 1.5). Since two suitable post shapes were already identified in **Figure 4a** for the size-based separation, the next steps were selecting specific designs from these two families and suitable ΔV values.

Figures 4b-4c contain the plots of $\Delta t_{R,p}$ between the blue and red particles (IDs # 6 and 5, $\Delta t_{R,p} = t_{R6,p} - \Delta t_{R5,p}$) for designs Square-Oval-VS20-HS100 and Oval-Square-VS20-HS100 at five distinct horizontal post lengths and as a function of the applied ΔV values, respectively. To ensure a size-based elution order, $\Delta t_{R,p}$ between particles IDs # 6 and 5 must be positive, requiring high ΔV values. An extra value of horizontal post length of 350 µm was studied, which had negligible to small impact on both configurations, thus, 300 µm horizontal post length was selected as the best option. The Oval-Square configurations require lower ΔV values to achieve the size-based elution order, i.e., positive $\Delta t_{R,p}$ values, thus, this post shape was selected over Square-Oval, as lower ΔV are advantageous. In summary, the selected design for the size-based separation was Oval-210-Square-90-VS20-HS100.

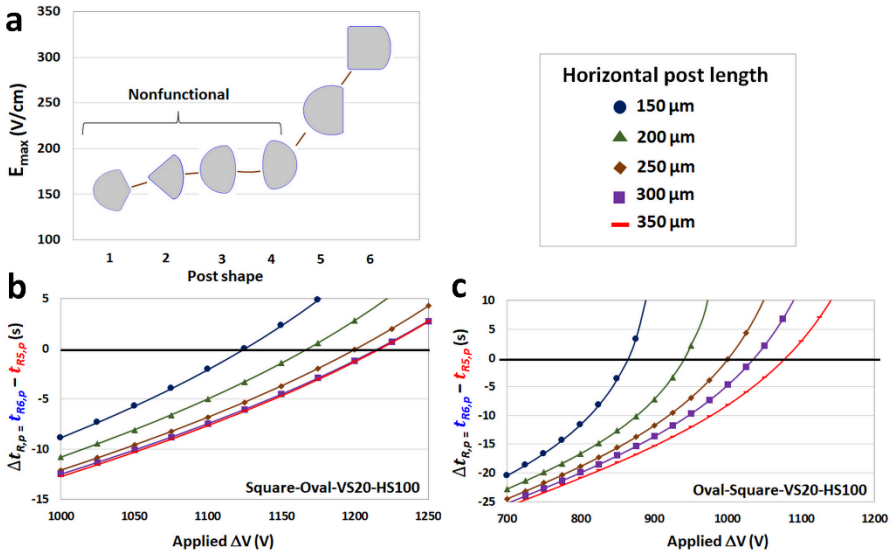

Figure 4. COMSOL predictions for the size-based separation under high voltages. **a)** Plot of the highest possible **E** for the six distinct post shapes, showing that only Square-Oval and Oval-Square configurations are suitable. **b-c)** Plots of $\Delta t_{R,p}$ values between particle IDs # 6 and 5 in Square-Oval-VS20-HS100 and Oval-Square-VS20-HS100 configurations with five distinct horizontal post lengths and as a function of the applied ΔV, respectively.

Experimental Sized-Based Separation of a Tertiary Sample Using the Improved Device

First, COMSOL simulations were employed to identify suitable voltages (**Table S4**) considering the design Oval-210-Square-90-VS20-HS100 (**Figure 5a**). The modeling results illustrated that a $\Delta V \geq 1050\,V$ (**E**≥ 213.0 V/cm) should produce a successful size-based separation with particles eluting in the following order: green, red and blue, as dictated by their size and $\mu_{EP,NL}^{(3)}$values. As discussed, larger particles sizes have a larger $\mu_{EP,NL}^{(3)}$ magnitudes.[26,38] The voltages selected for the experimental separation are listed in **Table 3**.

Initially, a $\Delta V = 1200\,V$ (**E**= 249.2 V/cm) was used, since simulations predicted trapping of the 11.7 µm blue particle above this voltage (**Table S4**). However, the experiments showed that a $\Delta V = 1500\,V$ (**E**= 321.7 V/cm) was required, i.e., the separation had overlapping peaks with $\Delta V < 1500\,V$. **Figure 5b-5c** show images of the particles migrating in the expected size-based order: green, red and blue, as predicted by COMSOL. **Table 4** shows that under $\Delta V = 1500\,V$, the $t_{R,e}$ values for the green, red, and blue particles are 50, 125, and 254 s, respectively, which shows a deviation < 27 % from COMSOL predictions ($t_{R,p}$) for green and red particles. No deviation was determined for the blue particles, since under $\Delta V = 1500\,V$, COMSOL predicted trapping of the blue particles. The COMSOL model is a useful tool, but it is not always perfect, as was discussed above. Good reproducibility was obtained between repetitions, as deviations are below 19 % (**Table 4**). This size-based is the result of a combination of linear and nonlinear phenomena, where EP_{NL} is the main discriminatory effect driving the separation. The velocity plots in **Figures S3d-f** for $\Delta V = 1200\,V$ and **Figures S3g-i** for $\Delta V = 1500\,V$ provide more details on the relative contributions of each one the four EK phenomena considered here.

This separation had resolutions of *Rs* = 3.06 between the green and red particles and *Rs* = 3.69 between the red and blue particles, illustrating complete separations (*Rs*>1.5) and the effectiveness of the proposed device design method. The number of plates per meter were 11,022, 7,246 and 37,614 plates/m for the green, red, and blue particles, respectively. For comparison, a design identified as "nonfunctional" was employed to perform the size-based separation, yielding poor separation results (**Fig. S4**).

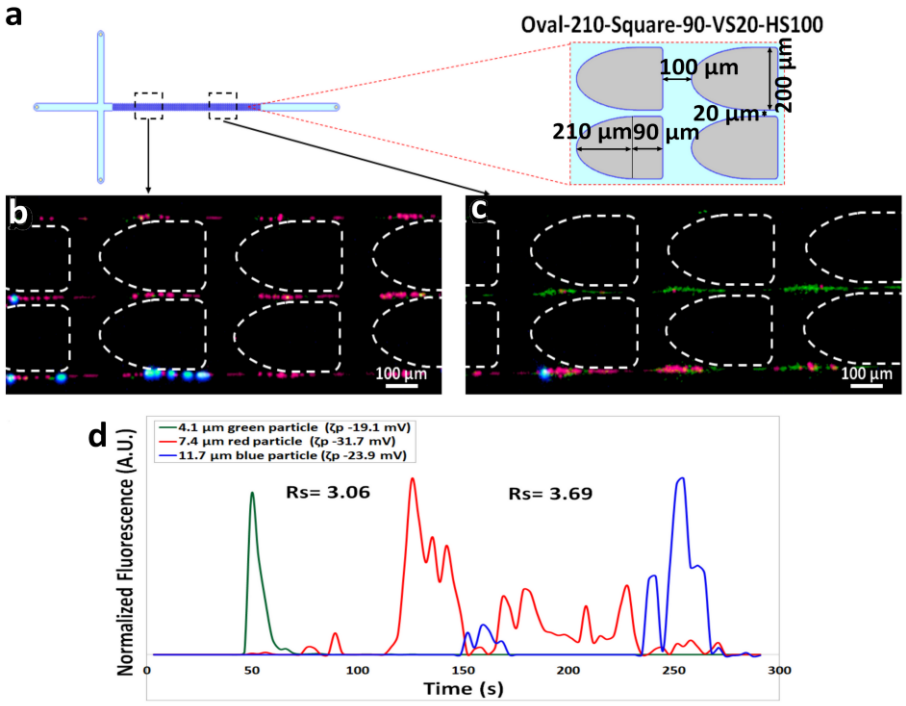

Figure 5. Experimental results for the size-based separation. **a)** Illustration of the device. **b-c)** Particles as they migrate across the post array in the following order: green first, then red, with the blue particles migrating last. **d)** Electropherogram depicting the three particle peaks. A video of this separation is included as supplementary information as **Video_S2.mp4**. Results were obtained under ΔV = 1500 V.

CONCLUSIONS

This study proposes a method for designing iEK systems for the continuous separation of tertiary microparticle samples based on charge and size differences. COMSOL *Multiphysics* enabled the prediction of particle retention with the primary of amplifying the differences in predicted particle retention times. Various configurations were explored with simulations, encompassing six shapes of insulating posts, six values of spacing between posts and four values of horizontal post length. Charge-based and size-based separations differ in the EK mechanisms responsible for driving the separation, charge-based separations are possible under EP_L effects, while size-based separations can be achieved under EP_{NL} effects. Results revealed that devices with Oval-Square shaped post were the most suited for charge-based separations, while devices with Oval-Square shaped posts were the best option for size based separations. These findings illustrate the potential of the device design method presented here for identifying effective device configurations for the separation of complex mixtures of microparticles, which can be extended to applications with microorganisms.

ASSOCIATED CONTENT

Supporting Information

The supplementary file contains **Tables S1-S5** and **Figures S1-S4**. Additionally, the video files **Video_S1.mp4**, **Video_S2.mp4** are also included. These videos depict simultaneously the elution of the particles and the acquisition of the fluorescence as a function of time.

AUTHOR INFORMATION

Corresponding Author

Email: bhlbme@rit.edu

ORCID

Blanca H. Lapizco-Encinas: 0000-0001-6283-8210

Author contributions

AVK: Experimentation, data analysis, writing original draft – review & editing. **PC:** Data analysis, writing original draft – review & editing. **BHLE:** Conceptualization, methodology, project administration, supervision, writing original draft – review & editing.

Notes:

The authors declare no competing financial interest.

ACKNOWLEDGMENTS

This material is based upon work supported by the National Science Foundation under Award No. 2127592.

REFERENCES

(1) Rajapaksha, P.; Elbourne, A.; Gangadoo, S.; Brown, R.; Cozzolino, D.; Chapman, J. A Review of Methods for the Detection of Pathogenic Microorganisms. *Analyst* **2019**, *144* (2), 396–411. https://doi.org/10.1039/C8AN01488D.

(2) Lapizco-Encinas, B. H. Microscale Nonlinear Electrokinetics for the Analysis of Cellular Materials in Clinical Applications: A Review. *Microchim. Acta* **2021**, *188* (3), 104. https://doi.org/10.1007/s00604-021-04748-7.

(3) Vaghef-Koodehi, A.; Lapizco-Encinas, B. H. Microscale Electrokinetic-Based Analysis of Intact Cells and Viruses. *Electrophoresis* **2022**, *43* (1–2), 263–287. https://doi.org/10.1002/elps.202100254.

(4) Ding, J.; Woolley, C.; Hayes, M. A. Biofluid Pretreatment Using Gradient Insulator-Based Dielectrophoresis: Separating Cells from Biomarkers. *Anal. Bioanal. Chem.* **2017**, *409* (27), 6405–6414. https://doi.org/10.1007/s00216-017-0582-5.

(5) Jones, P. V.; Salmon, G. L.; Ros, A. Continuous Separation of DNA Molecules by Size Using Insulator-Based Dielectrophoresis. *Anal. Chem.* **2017**, *89* (3), 1531–1539. https://doi.org/10.1021/acs.analchem.6b03369.

(6) Aghaamoo, M.; Aghilinejad, A.; Chen, X.; Xu, J. On the Design of Deterministic Dielectrophoresis for Continuous Separation of Circulating Tumor Cells from Peripheral Blood Cells. *Electrophoresis* **2019**, *40* (10), 1486–1493. https://doi.org/10.1002/elps.201800459.

(7) Lu, X.; Hsu, J. P.; Xuan, X. Exploiting the Wall-Induced Non-Inertial Lift in Electrokinetic Flow for a Continuous Particle Separation by Size. *Langmuir* **2015**, *31* (1), 620–627. https://doi.org/10.1021/la5045464.

(8) Calero, V.; Garcia-Sanchez, P.; Ramos, A.; Morgan, H. Combining DC and AC Electric Fields with Deterministic Lateral Displacement for Micro- And Nano-Particle Separation. *Biomicrofluidics* **2019**, *13* (5), 054110. https://doi.org/10.1063/1.5124475.

(9) Lewpiriyawong, N.; Yang, C. Continuous Separation of Multiple Particles by Negative and Positive Dielectrophoresis in a Modified H-Filter. *Electrophoresis* **2014**, *35* (5), 714–720. https://doi.org/10.1002/ELPS.201300429.

(10) Coll De Peña, A.; Miller, A.; Lentz, C. J.; Hill, N.; Parthasarathy, A.; Hudson, A. O.; Lapizco-Encinas, B. H. Creation of an Electrokinetic Characterization Library for the Detection and Identification of Biological Cells. *Anal. Bioanal. Chem.* **2020**, *412* (16), 3935–3945. https://doi.org/10.1007/s00216-020-02621-9.

(11) Gencoglu, A.; Olney, D.; Lalonde, A.; Koppula, K. S.; Lapizco-Encinas, B. H. Dynamic Microparticle Manipulation with an Electroosmotic Flow Gradient in Low-Frequency Alternating Current Dielectrophoresis. *Electrophoresis* **2014**, *35* (2–3), 362–373. https://doi.org/10.1002/elps.201300385.

(12) Lentz, C. J.; Hidalgo-Caballero, S.; Lapizco-Encinas, B. H. Low Frequency Cyclical Potentials for Fine Tuning Insulator-Based Dielectrophoretic Separations. *Biomicrofluidics* **2019**, *13* (4), 044114. https://doi.org/10.1063/1.5115153.

(13) Hill, N.; Lapizco-Encinas, B. H. Continuous Flow Separation of Particles with Insulator-Based Dielectrophoresis Chromatography. *Anal. Bioanal. Chem.* **2020**, *412* (16), 3891–3902. https://doi.org/10.1007/s00216-019-02308-w.

(14) Jellema, L. C.; Mey, T.; Koster, S.; Verpoorte, E. Charge-Based Particle Separation in Microfluidic Devices Using Combined Hydrodynamic and Electrokinetic Effects. *Lab Chip* **2009**, *9* (13), 1914–1925. https://doi.org/10.1039/b819054b.

(15) Zhu, J.; Xuan, X. Curvature-Induced Dielectrophoresis for Continuous Separation of Particles by Charge in Spiral Microchannels. *Biomicrofluidics* **2011**, *5* (2), 24111. https://doi.org/10.1063/1.3599883.

(16) Patel, S.; Qian, S.; Xuan, X. Reservoir-Based Dielectrophoresis for Microfluidic Particle Separation by Charge. *Electrophoresis* **2013**, *34* (7), 961–968. https://doi.org/10.1002/elps.201200467.

(17) Hill, N.; Lapizco-Encinas, B. H. On the Use of Correction Factors for the Mathematical Modeling of Insulator Based Dielectrophoretic Devices. *Electrophoresis* **2019**, *40* (18–19), 2541–2552. https://doi.org/10.1002/elps.201900177.

(18) LaLonde, A.; Gencoglu, A.; Romero-Creel, M. F.; Koppula, K. S.; Lapizco-Encinas, B. H. Effect of Insulating Posts Geometry on Particle Manipulation in Insulator Based Dielectrophoretic Devices. *J. Chromatogr. A* **2014**, *1344*, 99–108. https://doi.org/10.1016/j.chroma.2014.03.083.

(19) Saucedo-Espinosa, M. A.; Lapizco-Encinas, B. H. Design of Insulator-Based Dielectrophoretic Devices: Effect of Insulator Posts Characteristics. *J. Chromatogr. A* **2015**, *1422*, 325–333. https://doi.org/10.1016/j.chroma.2015.10.030.

(20) Khair, A. S. Nonlinear Electrophoresis of Colloidal Particles. *Current Opinion in Colloid and Interface Science*. Elsevier March 25, 2022, p 101587. https://doi.org/10.1016/j.cocis.2022.101587.

(21) Rouhi Youssefi, M.; Diez, F. J. Ultrafast Electrokinetics. *Electrophoresis* **2016**, *37* (5–6), 692–698. https://doi.org/10.1002/elps.201500392.

(22) Tottori, S.; Misiunas, K.; Keyser, U. F.; Bonthuis, D. J. Nonlinear Electrophoresis of Highly Charged Nonpolarizable Particles. *Phys. Rev. Lett.* **2019**, *123* (1), 14502. https://doi.org/10.1103/PhysRevLett.123.014502.

(23) Cardenas-Benitez, B.; Jind, B.; Gallo-Villanueva, R. C.; Martinez-Chapa, S. O.; Lapizco-Encinas, B. H.; Perez-Gonzalez, V. H. Direct Current Electrokinetic Particle Trapping in Insulator-Based Microfluidics: Theory and Experiments. *Anal. Chem.* **2020**, *92* (19), 12871–12879. https://doi.org/10.1021/acs.analchem.0c01303.

(24) Morrison, F. A. Electrophoresis of a Particle of Arbitrary Shape. *J. Colloid Interface Sci.* **1970**, *34* (2), 210–214. https://doi.org/10.1016/0021-9797(70)90171-2.

(25) Li, D. Electrophoretic Motion of Particles in Microchannels. In *Interface Science and Technology*; 2004; Vol. 2, pp 542–616. https://doi.org/10.1016/S1573-4285(04)80031-0.

(26) Ernst, O. D.; Vaghef-Koodehi, A.; Dillis, C.; Lomeli-Martin, A.; Lapizco-Encinas, B. H. Dependence of Nonlinear Electrophoresis on Particle Size and Electrical Charge. *Anal. Chem.* **2023**, *95* (16), 6595–6602. https://doi.org/10.1021/acs.analchem.2c05595.

(27) Lomeli-Martin, A.; Ernst, O. D.; Cardenas-Benitez, B.; Cobos, R.; Khair, A. S.; Lapizco-Encinas, B. H. Characterization of the Nonlinear Electrophoretic Behavior of Colloidal Particles in a Microfluidic Channel. *Anal. Chem.* **2023**, *95* (16), 6740–6747. https://doi.org/10.1021/acs.analchem.3c00782.

(28) Bentor, J.; Dort, H.; Chitrao, R. A.; Zhang, Y.; Xuan, X. Nonlinear Electrophoresis of Dielectric Particles in Newtonian Fluids. *Electrophoresis* **2023**, *44* (11–12), 938–946. https://doi.org/10.1002/elps.202200213.

(29) Antunez-Vela, S.; Perez-Gonzalez, V. H.; Coll De Peña, A.; Lentz, C. J.; Lapizco-Encinas, B. H. Simultaneous Determination of Linear and Nonlinear Electrophoretic Mobilities of Cells and Microparticles. *Anal. Chem.* **2020**, *92* (22), 14885–14891. https://doi.org/10.1021/acs.analchem.0c03525.

(30) Vaghef-Koodehi, A.; Dillis, C.; Lapizco-Encinas, B. H. High-Resolution Charge-Based Electrokinetic Separation of Almost Identical Microparticles. *Anal. Chem.* **2022**, *94* (17), 6451–6456. https://doi.org/10.1021/acs.analchem.2c00355.

(31) Vaghef-Koodehi, A.; Ernst, O. D.; Lapizco-Encinas, B. H. Separation of Cells and Microparticles in Insulator-Based Electrokinetic Systems. *Anal. Chem.* **2023**, *95* (2), 1409–1418. https://doi.org/10.1021/acs.analchem.2c04366.

(32) Saucedo-Espinosa, M. A.; Lapizco-Encinas, B. H. Refinement of Current Monitoring Methodology for Electroosmotic Flow Assessment under Low Ionic Strength Conditions. *Biomicrofluidics* **2016**, *10* (3), 033104. https://doi.org/10.1063/1.4953183.

(33) Miller, A.; Hill, N.; Hakim, K.; Lapizco-encinas, B. H. Fine-tuning Electrokinetic Injections Considering Nonlinear Electrokinetic Effects in Insulator-based Devices. *Micromachines* **2021**, *12* (6), 628. https://doi.org/10.3390/mi12060628.

(34) Perez-Gonzalez, V. H.; Gallo-Villanueva, R. C.; Cardenas-Benitez, B.; Martinez-Chapa, S. O.; Lapizco-Encinas, B. H. Simple Approach to Reducing Particle Trapping Voltage in Insulator-Based Dielectrophoretic Systems. *Anal. Chem.* **2018**, *90* (7), 4310–4315. https://doi.org/10.1021/acs.analchem.8b00139.

(35) Beckman, J.; Song, Y.; Gu, Y.; Voronov, S.; Chennamsetty, N.; Krystek, S.; Mussa, N.; Li, Z. J. Purity Determination by Capillary Electrophoresis Sodium Hexadecyl Sulfate (CE-SHS): A Novel Application For Therapeutic Protein Characterization. *Anal. Chem.* **2018**, *90* (4), 2542–2547. https://doi.org/10.1021/acs.analchem.7b03831.

(36) Breadmore, M. C. Electrokinetic and Hydrodynamic Injection: Making the Right Choice for Capillary Electrophoresis. *Bioanalysis*. Future Science Ltd 2009, pp 889–894. https://doi.org/10.4155/bio.09.73.

(37) Saucedo-Espinosa, M. A.; Lapizco-Encinas, B. H. Exploiting Particle Mutual Interactions To Enable Challenging

Dielectrophoretic Processes. *Anal. Chem.* **2017**, *89* (16), 8459–8467. https://doi.org/10.1021/acs.analchem.7b02008.

(38) Dukhin, S. S. Electrokinetic Phenomena of the Second Kind and Their Applications. *Adv. Colloid Interface Sci.* **1991**, *35* (C), 173–196. https://doi.org/10.1016/0001-8686(91)80022-C.

Graphical abstract (TOC)